Development and Characterization of Organic Electronic Scaffolds for Bone Tissue Engineering

Iandolo, Donata; Ravichandran, Akhilandeshwari; Liu, Xianjie; Wen, Feng; Chan, Jerry K. Y.; Berggren, Magnus; Teoh, Swee-Hin; Simon, Daniel T.

2016

Iandolo, D., Ravichandran, A., Liu, X., Wen, F., Chan, J. K. Y., Berggren, M., et al. (2016). Development and Characterization of Organic Electronic Scaffolds for Bone Tissue Engineering. Advanced Healthcare Materials, 5(12), 1505-1512.

https://hdl.handle.net/10356/80765

https://doi.org/10.1002/adhm.201500874

DOI:

Article type: Full Paper

Development and characterization of organic electronic scaffolds for bone tissue engineering

Donata Iandolo[*#], *Akhilandeshwari Ravichandran*[#], *Xianjie Liu, Feng Wen, Jerry K.Y. Chan, Magnus Berggren, Swee-Hin Teoh, Daniel T. Simon*[*]

Dr. D. Iandolo., Prof. M. Berggren., Dr. D.T. Simon.

Laboratory of Organic Electronics, Department of Science and Technology, Linköping University, Norrköping SE-601 74, Sweden.

donata.iandolo@liu.se, daniel.simon@liu.se

A. Ravichandran, Dr. F. Wen., Prof. S.H. Teoh.

School of Chemical and Biomedical Engineering, Nanyang Technological University, 637459, Singapore.

Dr. X. Liu.

Department of Physics, Chemistry and Biology, Linköping University, Linköping, SE-581 83, Sweden.

Prof. J.K.Y. Chan.

Department of Obstetrics and Gynaecology, Yong Loo Lin School of Medicine, National University of Singapore, Singapore, 119077; Department of Reproductive Medicine, KK Women's and Children's Hospital, 229899, Singapore; Cancer and Stem Cell Biology Program, Duke-NUS Graduate Medical School, 169857, Singapore.

[#] These authors contributed equally to this paper.

[*] Corresponding authors

Keywords: Bioelectronics, Stem cells, Tissue engineering, 3D scaffolds

Abstract

Bones have been shown to exhibit piezoelectric properties, responding to electrical stimulation and generating electrical potential upon mechanical deformation. Thus, significant research has been devoted to study the effects of electrical stimulation on bone tissue engineering. However, in bone regeneration applications, only few studies have focused on the use of electroactive 3D biodegradable scaffolds and the effects on stem cells compatibility. Here a method is described to combine the bone regeneration capabilities of 3D-printed macroporous medical grade polycaprolactone (PCL) scaffolds with the electrical and electrochemical capabilities of the conducting polymer poly(3,4-ethylenedioxythiophene) (PEDOT). PCL scaffolds have been shown to be highly effective *in vivo* as bone regeneration grafts, and PEDOT is a leading material in the field of organic bioelectronics, due to its stability, conformability, and biocompatibility. A protocol is reported for scaffolds functionalization with PEDOT, using vapor-phase polymerization, resulting in a conformal conducting layer. Scaffolds' porosity as well as mechanical stability, important for *in vivo* bone regeneration applications, are retained. Human fetal mesenchymal stem cells proliferation is assessed on the functionalized scaffolds, showing the cytocompatibility of the polymeric coating. Altogether, these results show the feasibility of the proposed approach to obtain electroactive scaffolds for electrical stimulation of stem cells for applications in regenerative medicine.

1. Introduction

Efforts in tissue regeneration have benefited significantly from the development and availability of tailored 3D scaffolding. In particular, scaffolds prepared via the 3D printing technique of fused

deposition modelling (FDM) are both readily-accessible and of great utility.[1] Extensive work has been devoted at improving the properties of these FDM-based scaffolds to determine optimal porosity and pore dimension (important for cell ingrowth, oxygen diffusion, and waste product removal), the best materials or composites (for example, to optimize scaffold integration/resorption and degradation time), and surface functionalities.[1d] Several studies have identified polycaprolactone (PCL) as a viable material for 3D macroporous tissue regeneration scaffolds, specifically for bone regeneration. PCL-based scaffolds prepared by FDM have been applied both *in vitro* and *in vivo*, demonstrating their efficacy as bone regeneration grafts in critical-size defects.[2] Moreover, PCL macroporous scaffolds have proven to be highly versatile as 3D cell-growth substrates in a variety of culture conditions, from small-scale culturing up to lab-scale bioreactors.[3] 3D cell cultures in bioreactor are very beneficial to cell populations since they provide a dynamic culture environment enhancing mass transfer also within the internal pores of the 3D scaffolds, in particular important for the thick scaffolds employed in orthopaedics. Zhang and coworkers reported the use of a biaxial bioreactor for human fetal mesenchymal stem cells culture for the development of effective tissue-engineered bone graft (TEBG).[3a] They showed that TEBG primed with human fetal mesenchymal stem cells (hfMSC) induced higher volume of bone formation, with better structural properties compared to the acellular scaffold. Furthermore, they showed that only the animals transplanted with the hfMSC-TEBG underwent full fracture repair of critical-sized bone defects.[2a] Human fetal MSCs (hfMSCs) have been shown to exhibit the most proliferation and osteogenic capacity, as well as the least immunogenicity, suggesting they are superior candidates for bone tissue engineering.[2a, 4]

Before the work by Fukada and Yasuda about bone piezoelectricity, it was well known that mechanical stresses can remodel bones and that mechanical strain is required to maintain bone architecture.[5] However the relationship between the mechanical stress and piezoelectric potentials *in vivo* was not clear,[6] and the subsequent discovery of piezoelectricity in bones has prompted several investigations of the interplay between electrical stimulation and bone regeneration.[1b, 7] Thus

combining the regenerative efficacy of PCL-based scaffolds with the possibility to actively influence cell differentiation and behavior by electrical stimulation is of great interest and potential. With this aim in mind, one straightforward option is to supplement existing scaffolds with electrical and electrochemical conductivity.

A variety of electrically conductive materials have been explored at the interface with cells and tissue, such as metals, graphene, carbon nanotubes, and conductive conjugated polymers.[8] Conductive layers can be obtained by depositing a thin film or conductive polymer layer on flat surfaces as well as 3D-structured features.[9] For example, our group showed that polyethylene terephthalate (PET) nanofibers could be coated via vapor-phase polymerization (VPP) with the well-known conducting polymer poly(3,4-ethylenedioxythiophene) (PEDOT).[9a, 10] The coated fibers maintained their morphology and were used to grow and electrically stimulate neuronal cells. In bone regeneration applications, only a limited number of studies have been published on the use of biocompatible electroactive 3D scaffolds for electrical stimulation. Shahini et al. reported the use of PEDOT as the conductive material in a blend with gelatin and bioactive glass, assessing the scaffolds' cytocompatibility using adult hMSC.[11] Jin and Kim used scaffolds prepared by 3D printing a blend of PCL and β-tricalcium phosphate (β-TCP) for electrical stimulation of osteoblasts (via external electrodes).[1b] Both calcium deposition and alkaline phosphatase (ALP) activity were positively affected by electrical stimulation, although the main cause seemed to be the release of β-TCP triggered by the electric field. Pelto and coworkers investigated the effect of electrical stimulation of human adipose stem cells (hASC) using biodegradable 3D scaffolds coated with chondroitin sulfate-doped polypyrrole (PPy).[12] They observed enhanced hASC proliferation, but did not see a significant difference on active electrical stimulation, possibly due to chondroitin sulfate-doped coating providing the dominant effect. However, to the best of the writers' knowledge the use of PEDOT as electrically and electrochemically active substrate for human fetal mesenchymal stem cells has not been reported before.

Based on the tissue regeneration efficacy of PCL macroporous scaffolds, and the concomitant rise of PEDOT as a conducting polymer-of-choice for bioelectronics applications,[13] we endeavored in this study to combine these two material platforms. The aim was to create a tool for bone regeneration that preserves PCL scaffolds' cell proliferation properties, while supplementing the 3D structures with electrical addressability for future electrically-stimulated regeneration studies. The resulting PEDOT-coated PCL scaffolds were assessed morphologically, chemically, and electrochemically. This study also evaluated the cytocompatibility of this newly-developed platform with fetal mesenchymal stem cells (MSCs), a potent source of stem cells with high osteogenic potential.

2. Results

2.1 Characterization of the chemical composition of the PEDOT-coated PCL scaffolds.

Vapor phase polymerization (VPP) was chosen to deposit a continuous conductive PEDOT film on the 3D macroporous scaffolds while preserving their morphological cues. Compared to other coating techniques such as the chemical polymerization, VPP has been reported to guarantee both intended effects.[9a] For PEDOT polymerization, VPP is traditionally performed by addition of pyridine, a weak base, to the oxidant solution to reduce the oxidant reactivity, slowing down the polymerization process, thus achieving a more regular polymer film. Recently, the triblock copolymer PEG-PPG-PEG (PPP, 58000 Da) has been adopted as an alternative to pyridine.[14] Indeed, it has been proposed that triblock copolymers, like PEG-PPG-PEG, aid the polymerization process by suppressing iron(tosylate) crystallite formation, while simultaneously guiding PEDOT structuring and coordinating water supposedly involved in the reaction as proton scavenger.[15]

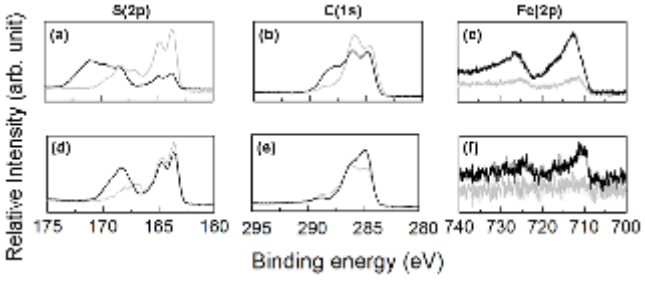

Figure 1. Chemical composition of the PEDOT:Tos layers. XPS spectra of the Pyr-PEDOT:Tos scaffolds (a-c) and PPP-PEDOT:Tos scaffolds (d-f). Samples were analyzed before (black line) and after (grey line) overnight rinsing in butanol.

In the present study, two solutions containing either pyridine or the triblock copolymer were used to fabricate the PEDOT:Tos coated scaffolds, denoted as Pyr-PEDOT:Tos or PPP-PEDOT:Tos, respectively. The polymerization occurs via oxidation of two EDOT monomers and with the concomitant electron transfer to iron passing from Fe(III) to Fe(II)). The resulting radicals on the oxidized EDOT lead to dimerization, and subsequent oligomerization with additional oxidized EDOT monomers.

The PEDOT layers were analyzed via FTIR and X-ray photoelectron spectroscopy (XPS). FTIR spectra were acquired on VPP PEDOT:Tos films prepared on undoped silicon wafers. In fact, it was not possible to characterize the macroporous scaffolds due to their discontinuous structure in either transmission or horizontal attenuated total reflectance (HATR) modes. FTIR spectra showed the presence of the peaks characteristic of PEDOT, demonstrating the successful deposition of the conjugated conductive polymer during the VPP process (Supporting Information, Figure S1).[16] XPS was used to ascertain the surface chemical composition of the coated 3D scaffolds and the effectiveness of the rinsing steps in removing excess of iron and tosylate ions, potentially cytotoxic. With XPS, we could discriminate the different contributions of the single components (PEDOT, Tosylate, and iron) and derive important information for characterizing both the coating process and the resulting PEDOT layers. In the PEDOT:Tos XPS spectrum, one can distinguish the S(2p) signals from the tosylate ions' sulphonate group (166 - 170 eV) and the thiophene units in PEDOT (163 - 166 eV),[17] as well the C(1s) signals from the C-C (285 eV), C-S (285.5 eV), and C-O-C (286.4 eV) bonds on the PEDOT chains and the triblock copolymer.[18] The S(2p) spectra of PPP-PEDOT:Tos (Figure 1a) indicate that the surface consisted mainly of tosylate-containing compounds, being effectively removed with the rinsing step. After extensive rinsing, a decrease in the peak at 288.06

eV was observed (Figure 1b), indicating that the content of triblock copolymer on the surface was reduced (Figure S2). The rinsing step was also effective in removing excess iron (Figure 1c). The XPS spectra for Pyr-PEDOT:Tos films (Figure 1d-f) likewise indicated efficient removal of excess tosylate ions and iron.

2.2 Characterization of the surface properties of PEDOT:Tos coated PCL scaffolds

Following VPP, continuous PEDOT layers surrounding the scaffold filaments were obtained (Figure 2), preserving the macroporosity typical of the 3D scaffolds (Figure 2 a-f) and which is beneficial for cells infiltration, waste product removal, and eventual vascularization. The VPP-processed scaffolds exhibited a rougher surface compared to the untreated ones. A slightly smoother and more homogeneous layer was achieved using the triblock copolymer instead of pyridine in the oxidant solution (Figure 2g-i). Both coating protocols resulted in an overall increase of surface roughness compared to the untreated PCL scaffolds, with the pyridine inducing the formation of larger areas of rough polymer (Figure 2i).

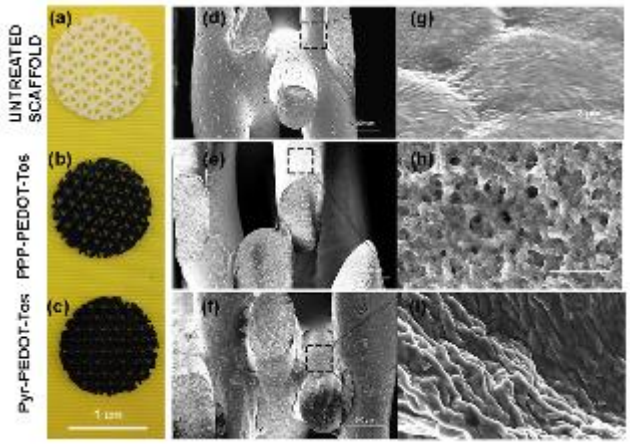

Figure 2. Scaffolds surface structure. Pictures of the uncoated and coated scaffolds and SEM images of the macroporous scaffolds before (a, d, g) and after VPP using the two different oxidant solutions. PPP-PEDOT:Tos scaffolds(b, e, h) and Pyr-PEDOT:Tos (c, f, i). (a-c: scale bar: 1cm, d-f: scale bar: 200 μm, g-i: scale bar: 2 μm).

The PEDOT:Tos coatings were also characterized using contact mode AFM (Fig. 3), clearly showing the increase in the surface rugosity due to the deposition of PEDOT:Tos, with a significant difference between the two oxidant solutions. The average roughness values (Ra) were estimated scanning 5 µm x 5 µm areas. The untreated scaffolds exhibit Ra = 16 ± 5 nm compared to Pyr-PEDOT:Tos (63 ± 10 nm), or PPP-PEDOT:Tos (38 ± 2 nm). The different kinetics and mechanisms of action of the two additives, pyridine and the triblock copolymer, added to the oxidant solution may account for the different morphologies of the formed PEDOT films (Figures 2 and 3). Surface roughness and topography have been showed to be important for effective cell attachment to the scaffolds, influencing proliferation and differentiation.[19]

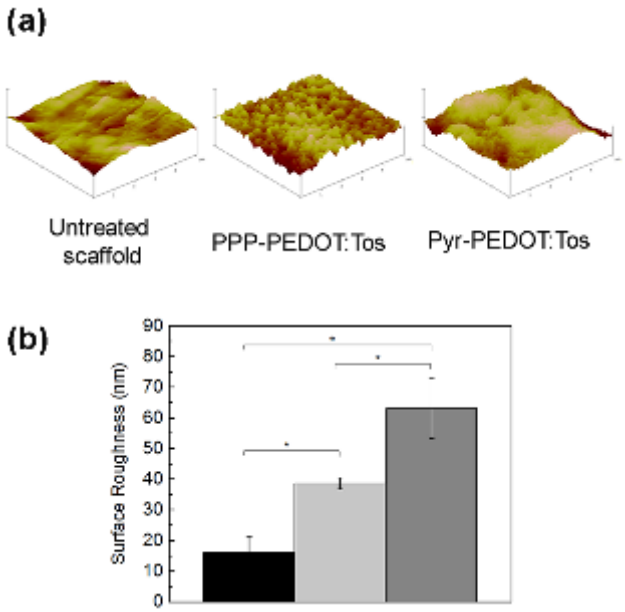

Figure 3. AFM analysis of untreated and PEDOT-Tos-coated scaffolds. (a) 3D rendered images of untreated, and PPP-PEDOT:Tos and Pyr-PEDOT:Tos coated scaffolds. Scanned area: 5 µm x 5 µm. (b) Ra values calculated for the uncoated PCL scaffolds (black bar) compared to those coated PPP-PEDOT:Tos (light grey) and Pyr-PEDOT-Tos (dark grey). *: the difference between data is statistically significant for $p < 0.05$.

Three different levels of surface roughness can be distinguished, depending on the dimensions of the features: macro-roughness (100 μm – mm), micro-roughness (100 nm – 100 μm), and nano-roughness (less than 100 nm). Macro-roughness has been reported to be beneficial for the anchorage of implants in the body. The effect of micro-roughness on cell proliferation and differentiation is more controversial, with several authors reporting an increased level of osteoblastic differentiation for cells cultured on micro-rough scaffolds.[19b-d] Nanoscale features have been shown to play a key role in the first stages of cell adhesion and subsequent proliferation.[20] It has been proposed that the various protein components of the extracellular matrix selectively bind to structures with increasing roughness. Due to particular stereochemical structures, proteins will preferentially adsorb to the features with the most appropriate dimensions.[20a]

As for the surface wettability, being the scaffolds highly porous (70 %), an accurate determination of the influence of the electroactive coating on the water contact angle of the scaffolds is not straightforward. Wettability properties were thus determined using planar PCL films coated with PEDOT:Tos, following the same procedures applied for the macroporous scaffolds. Coating PCL films with PEDOT:Tos resulted in a significant reduction in the water contact angle for PPP-PEDOT:Tos (11° ± 3°) and for Pyr-PEDOT:Tos (26° ± 5°), compared to the hydrophobic untreated PCL film (82° ± 5°) (Fig. 4a). It has been reported in literature that the presence of the PEDOT layer endows the coated surfaces with a hydrophilic character,[21] and the presence of PEG enhances this feature.[22] This increased wettability of the coated scaffolds can be beneficial for cell culture, as Jeon and colleagues reported a higher level of protein adsorption for macroporous 3D PCL scaffolds with increased roughness and wettability.[1c]

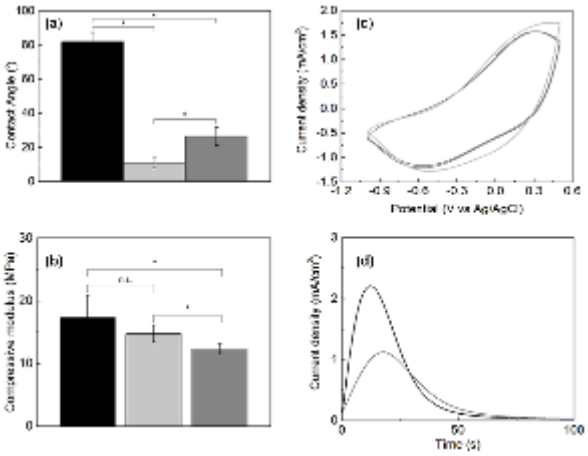

Figure 4. Scaffolds physical and electrochemical characterization. Water contact angle (a), compressive modulus (b), cyclic voltammetry (c) and charge storage ability (d) of the uncoated (black) and PPP-PEDOT:Tos (light grey) or Pyr-PEDOT:Tos (dark grey) coated scaffolds. The significance level was set at $p < 0.05$ when evaluating contact angle and the compressive modulus. *: the difference between data is statistically significant, n.s.: the difference between the two set of data is not statistically significant. Cyclic voltammetry experiments were run in NaTos 0.1M (pH: 5) at 20 mV s^{-1} using Ag/AgCl (3 M NaCl) as reference electrode and Pt mylar as counter electrode.

2.3 Analysis of mechanical properties

Mechanical properties were evaluated running compressive tests orthogonally to the scaffolds' surface (Figure 4b). The obtained values are in general slightly lower than those reported for other 3D scaffolds prepared via 3D printing using the same lay-down pattern (0/60/120°).[1a, 23] This difference in Young's modulus can be attributed to the different thickness of the samples used in the present compression studies compared to previously reported scaffolds. As compared to the untreated scaffolds, PPP-PEDOT:Tos scaffolds showed an almost unaffected compressive modulus (14.8 ± 1.4 MPa) compared to the untreated scaffolds (17.3 ± 3.6 MPa). Pyr-PEDOT:Tos, instead, showed a compressive modulus of 12.3 ± 0.9 MPa at $p < 0.05$.

2.4 Electrochemical characterization of the PEDOT coated 3D PCL scaffolds

Electrical characterization of the two different films was carried out using 4-probe measurements on thin film analogs on glass substrates (Supporting Information). Films prepared using the PPP instead of the pyridine resulted in higher electrical conductivity. Cyclic voltammetry experiments confirmed the electrochemical activity of the PEDOT:Tos films deposited on the scaffolds (Figure 4c). Both PPP-PEDOT:Tos and Pyr-PEDOT:Tos films present oxidation peaks (0.3 V) and reduction peaks (broad peak between –0.4 and 0.7 V). The redox peak positions broadly correlate with data available in literature.[21, 24] The shape of the CV spectra, however, differs when it is run on the scaffolds instead of planar gold electrodes (Figure S6). The difference in the shape of the recorded CVs may be attributed to the different thicknesses of the film obtained on the two substrates: glass and PCL scaffolds. Thicker and more porous films may lead to the formation of double layers during the redox process. Moreover, it has been reported the pH influences the position of the redox peaks. The experiments reported in Figure 4c were run at pH 5 instead of pH 6.9 as reported by others.[21]

The current density was recorded for 100 s and the charge storage ability was determined as the area under the charge density vs. time curve (Figure 4d). PPP-PEDOT:Tos scaffolds showed a higher charge capacity (54.6 ± 8.4 mA/cm^2) compared to Pyr-PEDOT:Tos (37.5 ± 8.5 mA/cm^2). The thicker film obtained using the triblock copolymer in the oxidant solution (Figure S7b) may account for the estimated higher current density, compared to the thinner layer obtained using pyridine (Figure S7c). The thicknesses of PPP-PEDOT:Tos and Pyr-PEDOT:Tos layers were calculated from SEM images of the cross sections of the coated macroporous scaffolds. PEDOT films were found to be 2.38 ± 0.38 µm for PPP-PEDOT:Tos and 0.37 ± 0.06 µm for Pyr-PEDOT:Tos. The oxidant solution including the triblock copolymer appears to show a higher viscosity as compared to the one containing pyridine. This higher viscosity may account for a higher coating efficiency for the triblock-containing solution. The differing morphologies observable in Fig. 2h and i may also contribute to the differences in overall PEDOT-layer thickness.

It should be added that given the higher porosity of the PPP-PEDOT:Tos samples, a higher fraction of the deposited polymer will be accessible for the electrolyte during the oxidation process thus guaranteeing a higher level of doping and thus stored charges.

2.5 PEDOT:Tos-coated scaffold cytocompatibility

Cytocompatibility studies were performed over 7 days by culturing hfMSCs on the uncoated and coated scaffolds. An increase in AlamarBlue® signal can be observed for all scaffolds at the three analyzed time points, with no statistical difference when compared to the uncoated ones, indicating increasing cellular metabolism over time in all cases (Figure 5a). These results highlight that the coating does not negatively affect the proliferation of the seeded cells. Phase contrast images and fluorescence microscopy images clearly show the spindle-shaped morphology of the mesenchymal stem cells and cellular occupancy in the scaffolds' pores (Figure 5b). From the results, compatibility of MSCs with the coated scaffolds was established, as demonstrated by the lack of PI (red stain), which is indicative of dead cells.

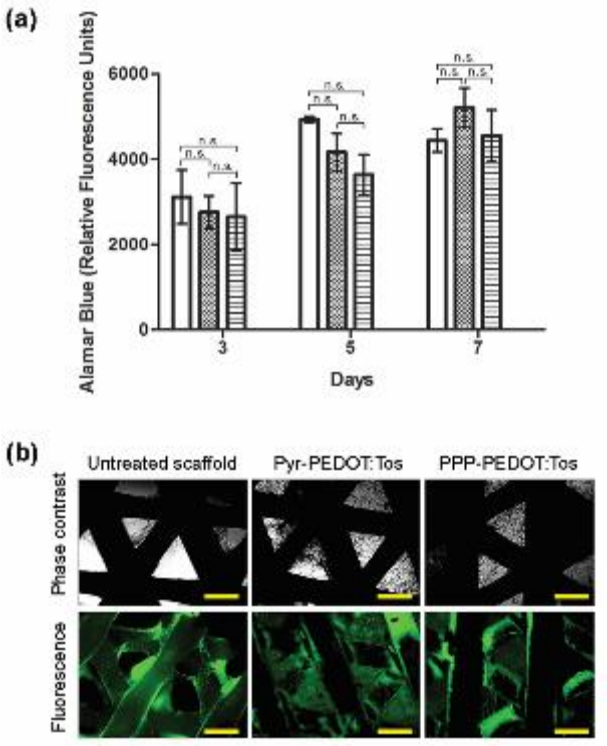

Figure 5. Mesenchymal stem cell proliferation on untreated and coated scaffolds. (a) Cellular metabolism on untreated (white bar), and Pyr-PEDOT:tos (squared bars) and PPP-PEDOT:Tos (striped bars) coated PCL scaffolds via AlamarBlue® assay ($p < 0.05$). n.s.: not significant difference. (b) Phase contrast microscopy and fluorescence microscopy images of hfMSCs (day 5 of culture) growing on untreated (a, d), and Pyr-PEDOT:tos (b, e) and PPP-PEDOT:Tos (c, f) coated PCL scaffolds. Scale bar 600 μm.

Scaffolds cytocompatibility over longer time span was assessed by evaluating hfMSCs proliferation up to day 14 from seeding (Figure S8). In addition, morphology of cells cultured on different scaffolds surfaces was investigated by performing F-actin staining at two time points (day 7 and day 14, figure 6). 3D confocal microscopy images were captured for cells growing on the scaffolds' struts. As it is possible to see in figure 6, after 7 days of cell proliferation cells colonized the scaffolds with no apparent difference among the different scaffolds typologies. Extensive actin fibers surrounding the struts and connecting cells can be observed.[25] Cells display a tridimensional arrangement of the actin fibers, typical of cells growing on 3D surfaces. Moreover, when comparing the two times points (day 7 and day 14), cells display the same extended tridimensional morphology suggesting no negative influence by any of the coating procedures on scaffolds colonization by the investigated cells also over a longer time span.

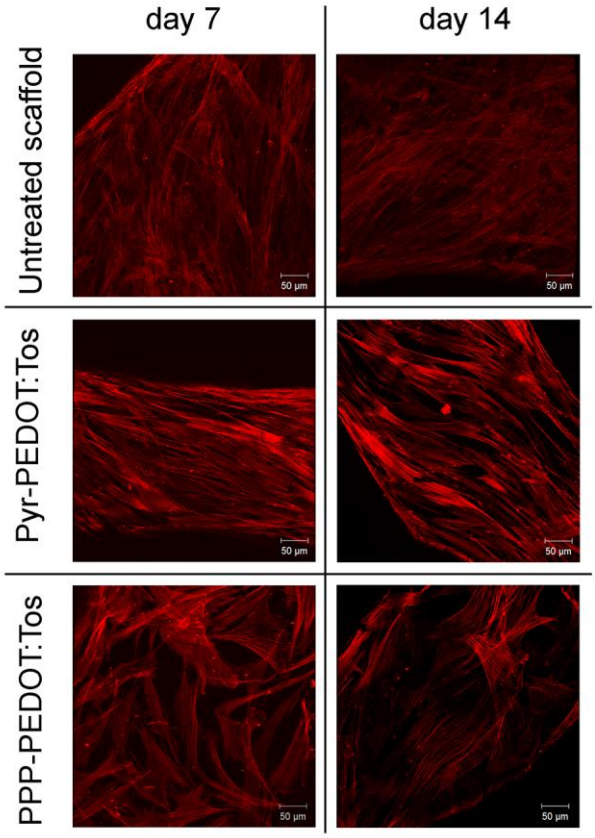

Figure 6. F-actin staining of fetal mesenchymal stem cells seeded on untreated and coated scaffolds. Z-stack images were taken for cells after 7 and 14 days of proliferation on different scaffolds surfaces. Scale bar: 50 µm.

3. Conclusions

We have developed a method to deposit a continuous, conformal layer of the electrically and electrochemically active polymer PEDOT on the 3D macroporous scaffolds. The VPP coating technique ensured adherent coating of the scaffolds' filaments without filling the voids of the porous structure. Preserving the porosity in this way is vital for subsequent cell culture as well as *in vivo* application; the voids allow for efficient transfer of nutrients and waste products to/from the cells, and allow cells to infiltrate and vascularize scaffolds once implanted *in vivo*. The PEDOT coatings also provided increased surface roughness and wettability, which have been shown to be beneficial for cell adhesion and proliferation. Chemical analysis of the coatings verified that potentially-cytotoxic excess iron and tosylate could be effectively removed, and indeed, hfMSCs seeded on the

scaffolds proliferated and seemed to be otherwise unaffected by the presence of the PEDOT during their growth over relevant time spans. While the mechanical properties were affected by the coating process, one of the protocols (using the triblock copolymer in the VPP oxidant solution, which also resulted in slightly better conductivity) produced reasonably strong coated scaffolds. These PEDOT-coated scaffolds are thus already comparable to PCL macroporous systems in terms of osteoinduction and therapeutic utility, but with the added functionality of electrical conductivity. They thus provide a new tool for the study and exploitation of electrically-augmented osteoinduction both in the lab and in the clinic.

4. Experimental section

Materials

3D printed macroporous medical grade PCL scaffolds with porosity of 70% were purchased from Osteopore^{TM}. Circular samples (12 mm diameter) were cut out of the 5 x 5 cm sheet using a metallic hole-puncher. PCL films (to be used for FTIR and contact angle measurements) were thermally pressed into a thickness of approximately 120 µm. Briefly, a known mass of PCL was placed between two stainless steel sheets on a Carver bench press (Carver Inc, USA). Temperature was elevated to 100 °C and pressure exerted for 30 min. The pressed film was then allowed to cool to room temperature via normal convection cooling.

Clevios™ CB 40 V2 (40% wt/wt Fe(III) p-toluenesulfonate (Tosylate) in butanol) was purchased from Heraeus (Germany). 3,4-Ethylenedioxythiophene (EDOT) monomer (142.18 g/mol), pyridine (79.10 g/mol), and the triblock copolymer poly(ethylene glycol)-block-poly(propylene glycol)-block-poly(ethylene glycol) (PEG-PPG-PEG, 5800 g/mol) were purchased from Sigma-Aldrich. All chemicals were used as received without further purification.

Vapor phase polymerization

The polymerization chamber has a cylindrical shape with a volume of 270 mL (h: 70 mm, d: 140 mm). The process was run at atmospheric pressure. The oxidant solutions contained Clevios™ CB 40 V2 diluted up to 20% wt/wt using butanol as solvent. Pyridine was added to the oxidant solution to a final concentration of 9.4 mM. In alternative experiments, PEG-PPG-PEG was added to a final concentration of 20% wt/wt using a mixture of butanol and water (3:1) to solubilize the different components. Samples were coated by first increasing surface wettability with UV ozone exposure (5 min each side) and then dipping into butanol. The samples were then immersed in the oxidant solution twice, with 50 °C bake for 2 min between each dipping step. Samples coated with the oxidant solutions were suspended inside the chamber, directly above a hot plate at 60 °C, and thereby exposed to EDOT vapors. Thus, a defined volume of EDOT is distributed on the glass slides at the bottom of the reaction chamber. After 4 hours in this configuration, samples were removed from the polymerization chamber, baked at 50 ºC for 10 min each side and rinsed in butanol, to get rid of the unreacted oxidant and EDOT monomers. Finally, samples were rinsed in deionized water to remove any trace of solvents and of iron and dried by flushing them with N_2.

Contact angle measurement

Optical contact angle was measured using an Optical Contact Angle and Surface Tension Meter CAM 200 (KSV Instruments) using 9 µl of deionized water. For these analyses, custom-made PCL films were used as substrates and pristine PCL was compared to VPP-coated films using the two oxidant solutions (containing either pyridine or triblock copolymer).

FTIR measurements

The surface chemistry of the PEDOT:Tos films was investigated using FTIR spectroscopy. FTIR measurements were run using an Equinox 55 spectrometer (Bruker). The samples used for FTIR analysis were PEDOT:Tos films (using either pyridine or triblock copolymer in the oxidant solution)

deposited via VPP on undoped silicon wafers (IR transparent), since it was not possible to get reliable FTIR spectra using the full PCL scaffolds.

X-ray photoelectron spectroscopy (XPS)

Macroporous scaffolds were investigated via X-ray photoelectron spectroscopy. Photoemission experiments were carried out using a Scienta ESCA 200 spectrometer in ultrahigh vacuum with a base pressure of 10^{-10} mbar. The measurement chamber was equipped with a monochromatic Al Kα X-ray source providing photons with 1486.6 eV for XPS. The XPS experimental condition was set so that the full width at half maximum of the clean Au $4f_{7/2}$ line was 0.65 eV. All spectra were collected at a photoelectron take-off angle of 0° (normal emission) at room temperature.

XPS spectra of the as-prepared samples were compared to those of the samples extensively rinsed in butanol and then eventually in distilled water.

Scanning electron microscopy

Morphological analysis of the structures was carried out by scanning electron microscopy (SEM) using a LEO 1550 Gemini field-emission scanning electron microscope (Leo, Zeiss, Germany). Images were acquired using an accelerating voltage of 5 kV using an aperture size of 2.4 mm. Unmodified PCL samples were coated with platinum via thermal evaporation. PEDOT:Tos coated scaffolds were not subjected to metal deposition, being intrinsically highly conductive.

Atomic force microscopy

Surface roughness was determined via atomic force microscopy on both the unmodified and PEDOT-coated PCL films and macroporous PCL scaffolds using a Dimension 3100 (Veeco). The average roughness (Ra) was determined by scanning 5 x 5 µm areas.

Mechanical properties

The influence of the coated layer and of the VPP process on the mechanical properties of the scaffolds was evaluated by compressive tests in the direction perpendicular to the sample surface. Samples were 12 mm wide and 1 mm thick. All the tests were carried out at a rate of 1 mm min^{-1} up to a strain of 0.5 mm mm^{-1} using an Instron testing system with a 5 kN load cell. Compressive modulus was determined from the linear part of the curves obtained for the unmodified and coated scaffolds.

Electrochemical characterization

Cyclic voltammetry (CV) experiments were run in NaTos 0.1 M (pH: 5) (bubbled with nitrogen for about 30 min prior to scanning) at 20 mV s^{-1}. Ag/AgCl (3 M NaCl) and Pt mylar were used as reference and counter electrodes, respectively. To this aim, PPP-PEDOT:Tos and Pyr-PEDOT:Tos coated macroporous scaffolds were glued to Au-coated PET sheets using conductive carbon paste. Attention was paid to coat the gold and the carbon paste with an insulating layer to prevent undesired electrochemical reactions. As a control, PEDOT films were deposited using the two oxidant solutions on gold-coated glass slides. These electrodes were used to run CV measurements in the same conditions as reported above. The charge storage ability was defined as the area under the charge density vs. time curve, recoded by applying 0.4 V over a period of 100 s, in the same buffer conditions as for the CV.

Cytocompatibility study

Mesenchymal stem cells (MSC) were isolated from fetal femurs as previously described [4] and maintained in Dulbecco's modified Eagle's medium (DMEM)-Glutamax (GIBCO, USA) supplemented with 10 % fetal bovine serum (FBS, Hyclone), 50 U/ml penicillin and streptomycin (GIBCO, USA), which will be referred to as D10 medium hereafter. The scaffolds were sterilized overnight using 90 % ethanol. Subsequently, the scaffolds were washed with distilled water and dried in the incubator. The dried scaffolds were seeded with MSCs using fibrin glue at a seeding density of

3000 cells/mm^3, and kept in the incubator for 1 h. Thereafter, 2 ml of D10 medium was added to the cell-seeded scaffolds. Cytocompatibility of the scaffolds was evaluated by measuring the proliferation of MSCs on the scaffolds at days 3, 5, and 7, using the AlamarBlue® assay kit. Culture medium was replaced with 500 μL D10 medium containing 50 μL (10 % v/v) of AlamarBlue® reagent, followed by incubation at 37 °C for 4 h. A 200-μL aliquot from each well was transferred into a 96-well plate and fluorescence was measured at 530 nm excitation wavelength and 590 nm emission wavelength.[19b] Qualitative analysis of cellular viability on the scaffolds was performed using phase contrast light microscopy (PCLM) and fluorescein diacetate/propidium iodide (FDA/PI, Life Technologies, Singapore) staining. FDA stains the viable cells green whereas PI stains the dead cells red. Stained cells were visualized using fluorescence microscopy (Olympus LX71, Japan).

Cell morphology study

F-actin staining was used to examine the morphology of cells attached on scaffolds surfaces. The staining was performed according to Li et al. with tetramethyl rhodamine isothiocyanate-conjugated phalloidin (1:500, Chemicon).[25a] Stained cells were visualized using confocal laser scanning microscopy (Zeiss LSM 510). Z-stack images were acquired to get the tridimensional distribution of the actin fibers surrounding the scaffolds' struts.

Ethics approval

Collection of human tissues for research purposes was approved by the Domain Specific Review Board of National Healthcare Group (DSRB-D-06-154), in compliance with international guidelines regarding the use of fetal tissue for research.[26]

Statistical analysis.

Statistical analysis was performed via one-way ANOVA using a significance level of $p < 0.05$. For the cytocompatibility study, data have been represented as mean ± SD and compared using student's t-test.

Supporting Information

Supporting Information is available from the Wiley Online Library or from the author.

Acknowledgements

The authors would like to thank Dan-Tiberiu Sbircea and Prof. Iain McCulloch for assistance with the GPC experiments, Dr. Dan Zhao for assistance with AFM, Sami Elhag for assistance with SEM and Dr. Jing Lim for his help in fabricating and quality control of the 3D printed scaffolds from Osteopore International Pte Ltd. We are also thankful to Innventia AB (Sweden) for running the mechanical tests. This research was funded by a Knut and Alice Wallenberg Foundation Scholar grant to Prof. Magnus Berggren (KAW 2012.0302) and the Nanyang Technological University Internal Funding (for AR, WF, TSH).

References

[1] a) J. H. Bae, H. R. Song, H. J. Kim, H. C. Lim, J. H. Park, Y. Liu, S. H. Teoh, *Tissue Eng. Part A* **2011**, *17*, 2389; b) G. H. Jin, G. H. Kim, *J. Mater. Chem. B* **2013**, *1*, 1439; c) H. J. Jeon, H. Lee, G. Kim, *Tissue Eng. Part. C Methods* **2014**, *20*, 951; d) M. Domingos, F. Intranuovo, T. Russo, R. D. Santis, A. Gloria, L. Ambrosio, J. Ciurana, P. Bartolo, *Biofabrication* **2013**, *5*, 045004.

[2] a) Z. Y. Zhang, S. H. Teoh, M. S. Chong, E. S. Lee, L. G. Tan, C. N. Mattar, N. M. Fisk, M. Choolani, J. Chan, *Biomaterials* **2010**, *31*, 608; b) A. Yeo, W. J. Wong, S. H. Teoh, *J. Biomed. Mater. Res. A* **2010**, *93*, 1358.

[3] a) Z. Y. Zhang, S. H. Teoh, E. Y. Teo, M. S. K. Chong, C. W. Shin, F. T. Tien, M. A. Choolani, J. K. Chan, *Biomaterials* **2010**, *31*, 8684; b) J. Rauh, F. Milan, K. P. Gunther, M. Stiehler, *Tissue Eng. Part B Rev.* **2011**, *17*, 263.

[4] Z. Y. Zhang, S. H. Teoh, M. S. K. Chong, J. T. Schantz, N. M. Fisk, M. A. Choolani, J. Chan, *Stem Cells* **2009**, *27*, 126.

[5] E. Fukada, I. Yasuda *J. Phys. Soc. Jpn.* **1957**, *12*, *1158*.

[6] C. A. Bassett, R. O. Becker, *Science* **1962**, *137*, 1063.

[7] a) M. T. Tsai, W. J. Li, R. S. Tuan, W. H. Chang, *J. Orthop. Res.* **2009**, *27*, 1169; b) I. S. Kim, J. K. Song, Y. L. Zhang, T. H. Lee, T. H. Cho, Y. M. Song, K. Kim, S. J. Kim, S. J. Hwang, *Biochim. Biophys. Acta* **2006**, *1763*, 907; c) I. S. Kim, J. K. Song, Y. M. Song, T. H. Cho, T.H. Lee, S. S. Lim, S. J. Kim, S. J. Hwang, *Tissue Eng. Part A* **2009**, *15*.

[8] a) J. Isaksson, P. Kjäll, D. Nilsson, N. Robinson, M. Berggren, A. Richter-Dahlfors, *Nat. Mater.* **2007**, *6*, 673; b) M. Asplund, T. Nyberg, O. Inganäs, *Polym. Chem.* **2010**, *1*, 1374; c) S. D. McCullen, J. P. Mcquilling, R. M. Grossfeld, J. L. Lubischer, L. I. Clarke, E. G. Loboa, *Tissue Eng. Part C Methods* **2010**, *16*, 1377.

[9] a) M. H. Bolin, K. Svennersten, X. Wang, I. S. Chronakis, A. Richter-Dahlfors, E. H. W. Jager, M. Berggren, *Sens. Actuator B-Chem.* **2009**, *142*, 451; b) S. Meng, Z. Zhang, M. Rouabhia, *J. Bone Miner. Metab.* **2011**, *29*, 535.

[10] L. Groenendaal, F. Jonas, D. Freitag, H. Pielartzik, J. R. Reynolds, *Adv. Mater.* **2000**, *12*, *481*.

[11] A. Shahini, M. Yazdimamaghani, K. J. Walker, M. A. Eastman, H. Hatami-Marbini, B. J. Smith, J. L. Ricci, S. V. Madihally, D. Vashaee, L. Tayebi, *Int. J. Nanomedicine* **2014**, *9*, 167.

[12] J. Pelto, M. Björninen, A. Pälli, E. Talvitie, J. Hyttinen, B. Mannerström, R. S. Seppanen, M. Kellomäki, S. Miettinen, S. Haimi, *Tissue Eng. Part A* **2013**, *19*, 882.

[13] a) R. M. Owens, G. G. Malliaras, *MRS Bulletin* **2010**, *35, 449;* b) G. Tarabella, F. M. Mohammadi, N. Coppedè, F. Barbero, S. Iannotta, C. Santato, F. Cicoira, *Chem. Sci.* **2013**, *4*, 1395; c) G. Lanzani, *Nature Mater.* **2014**, *13*, 775.

[14] a) M. V. Fabretto, D. R. Evans, M. Mueller, K. Zuber, P. Hojati-Talemi, R. D. Short, G. G. Wallace, P. J. Murphy, *Chem. Mater.* **2012**, *24*, 3998; b) M. Fabretto, C. Jariego-Moncunill, J. P. Autere, A. Michelmore, R. D. Short, P. Murphy, *Polymer* **2011**, *52*, 1725.

[15] a) K. Zuber, M. Fabretto, C. Hall, P. Murphy, *Macromol. Rapid Commun.* **2008**, *29*, 1503; b) M. Fabretto, K. Zuber, C. Hall, P. Murphy, *Macromol. Rapid Commun.* **2008**, *29*, 1403; c) M. Fabretto, K. Zuber, C. Hall, P. Murphy, H.J. Griesser, *J. Mater. Chem.* **2009**, *19*, 7871.

[16] S. V. Selvaganesh, J. Mathiyarasu, K. L. N. Phani, V. Yegnaraman, *Nanoscale Res. Lett.* **2007**, *2*, 546.

[17] O. Bubnova, Z. U. Khan, A. Malti, S. Braun, M. Fahlman, M. Berggren, X. Crispin, *Nature Mater.* **2011**, *10*, 429.

[18] a) T. Y. Kim, J. E. Kim, K. S. Suh, *Polym. Int.* **2006**, *55*, 80; b) T. Bala, R. D. Gunning, M. Venkatesan, J. F. Godsell, S. Roy, K. M. Ryan, *Nanotechnol.* **2009**, *20*, 415603.

[19] a) B. Vagaská, L. Bačáková, E. Filová, K. Balík, *Physiol. Res.* **2010**, *59*, 309; b) J. Y. Martin, Z.Schwartz,T. W. Hummert, D.M. Schraub, J. Simpson, J.J. Lankford, D. D. Dean, D. L. Cochran, B.D. Boyan, *J. Biomed. Mater. Res.* **1995**, *29*, 389; c) R. Olivares-Navarrete, S. L. Hyzy, M. E. Berg, J. M. Schneider, K. Hotchkiss, Z. Schwartz, B. D. Boyan, *Ann. Biomed. Eng.* **2014**, *42*, 2551; d) R. A. Gittens, T. Mclachlan, Y. Cai, S. Berner, R. Tannenbaum, Z. Schwartz, K. H. Sandhage, B. D. Boyan, *Biomaterials* **2011**, *32*, 3395.

[20] a) T. J. Webster, C. Ergun, R. H. Doremus, R. W. Siegel, R. Bizios, *J. Biomed. Mater. Res.* **2000**, *51*, 475; b) E. Palin, H.Liu, T. J. Webster, *Nanotechnol.* **2005**, *16*, 1828

[21] M. Bongo, O. Winther-Jensen, S. Himmelberger, X. Strakosas, M. Ramuz, A. Hama, E. Stavrinidou, G. G. Malliaras, A. Salleo, B. Winther-Jensen, R. M. Owens, *J. Mater. Chem. B* **2013**, *1*, 3860.

[22] V. Karagkiozaki, P. G. Karagiannidis, M. Gioti, P. Kavatzikidou, D. Georgiou, E. Georgaraki, S. Logothetidis, *Biochim.Biophys Acta* **2013**, *1830*, 4294.

[23] D. W. Hutmacher, T. Schantz, I. Zein, K. W. Ng, S. H. Teoh, K. C. Tan, *J. Biomed. Mater. Res. A* **2001**, *55*, 203.

[24] a) L. H. Jimison, A. Hama, X. Strakosas, V. Armel, D. Khodagholy, E. Ismailova, G. G. Malliaras, B. Winther-Jensen, R. M. Owens, *J. Mater. Chem.* **2012**, *22*, 19498; b) I. Gualandi, M. Marzocchi, E. Scavetta, M. Calienni, A. Bonfiglio, B. Fraboni, *J. Mater. Chem. B* **2015**, *2*, 6753; c) H. Tang, P. Kumar, S. Zhang, Z. Yi, G. D. Crescenzo, C. Santato, F. Soavi, F. Cicoira, *ACS Appl. Mater. Interfaces* **2015**, *7*, 969.

[25] a) H. Li, F. Wen, Y. S. Wong, F. Y. Boey, V. S. Subbu, D. T. Leong, K. W. Ng, G. K. L. Ng, L. P. Tan, *Acta Biomater.* **2012**, *8*, 531; b) E. Knight, S. Przyborski, *J. Anat.* **2015**, *227*, 746.

[26] M. S. K Chong, J. Lim, J. Goh, M. W. Sia, J. K.Y. Chan, S. H. Teoh, *Mol Pharm.* **2014**, *11*, 2126.